Designing a fully-compensated half-metallic ferrimagnet

Mario Žic,[1] Karsten Rode,[2] Naganivetha Thiyagarajah,[2] Yong-Chang Lau,[2] Davide Betto,[2] J.M.D. Coey,[2]
Stefano Sanvito,[2] Kerry J. O'Shea,[3] Ciaran A. Ferguson,[3] Donald A. MacLaren,[3] and Thomas Archer[1, *]

[1]*CRANN and School of Physics, Trinity College Dublin, Dublin 2, Ireland*
[2]*CRANN, AMBER and School of Physics, Trinity College Dublin, Dublin 2, Ireland*
[3]*SUPA, School of Physics & Astronomy, University of Glasgow, Glasgow G12 8QQ, United Kingdom*
(Dated: March 11, 2016)

Recent experimental work on Mn_2Ru_xGa demonstrates its potential as a compensated ferrimagnetic half-metal (CFHM). Here we present a set of high-throughput *ab initio* density functional theory calculations and detailed experimental characterisation, that enable us to correctly describe the nominal Mn_2Ru_xGa thin films, in particular with regard to site-disorder and defects. We then construct models that accurately capture all the key features of the Mn-Ru-Ga system, including magnetic compensation and the spin gap at the Fermi level. We find that electronic doping is necessary, which is achieved with a Mn/Ga ratio smaller than two. Our study shows how composition and substrate-induced biaxial strain can be combined to design a ferrimagnetic half-metal with a compensation point close to room temperature.

Compensated ferrimagnetic half metals (CFHM) have an ordered spin-state which results in an ordered spin state with no net magnetic moment. As the material creates no stray magnetic field it should have low Gilbert damping, and offer numerous advantages compared to standard ferromagnetic metals. These include higher frequency operation, higher packing density, reduced device power requirement and devices that are impervious to external magnetic fields. Although there is no net magnetic moment, the highly-polarised spin-state allows switching of the magnetisation via spin-transfer torque. The class of CFHMs was first envisaged by van Leuken and de Groot[1] in 1995, but despite significant effort[2–7] the goal of a CFHM had proved elusive.[8]

Recent experimental[9–11] and theoretical[12] efforts towards creating a CFHM have concentrated on the Heusler alloy system Mn_2Ru_xGa (MRG). Heusler alloys are made of four interlaced *fcc* lattices, which form a *bcc*-like structure. Mn_2RuGa has the full Heusler ($L2_1$) structure, with Mn occupying the $4a$ and $4c$ sites, Ru the $4d$ and Ga the $4b$ sites.[9] Half-metallic Heuslers with the $L2_1$ structure are expected to follow a modified Slater-Pauling curve with the net magnetic moment m given by $m = N_v - 24$ where N_v is the number of valence electrons. For Mn_2RuGa, $N_v=25$, resulting in a net moment of $1\,\mu_B$. Mn_2Ga was expected to have a half-Heusler ($C1_b$) structure,[13] with Mn on $4a$, $4c$ sites and Ga on $4b$ sites, thus leaving the $4d$ site empty. In half-metallic Heuslers with the $C1_b$ structure, the magnetic moment m is given by $m = N_v - 18$. For Mn_2Ga, $N_v = 17$ and hence $m = -1\,\mu_B$. The idea behind the Mn_2Ru_xGa system, as proposed by Kurt et al.[9], was that by changing the Ru content x a material can be formed mid-way between Mn_2RuGa and Mn_2Ga, that is half-metallic, yet presents no net magnetic moment.

Cubic Mn_2Ru_xGa was stabilized in thin film form by Kurt et al.[9], who showed that at $x \approx 0.5$ there is an ordered spin state with a critical temperature of approx-
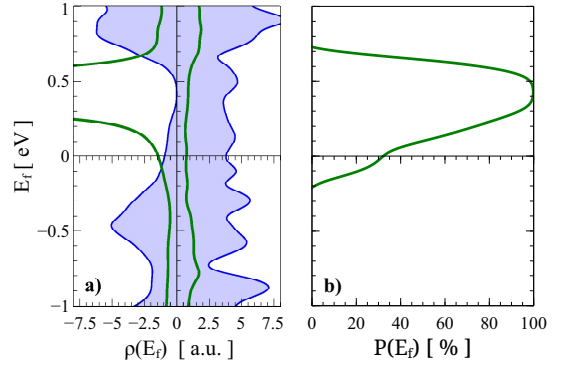

FIG. 1: a) Spin resolved resistivity (green) and the corresponding density of states (DOS) (blue) calculated for the $Mn_2Ru_{0.5}Ga$. The data corresponding to the spin down channel is represented with negative values. b) Calculated transport spin polarization.

imately $550\,K$ and a very small net magnetic moment. In the same work Andréev reflection (PCAR) spectroscopy showed a $54\,\%$ spin polarization at the Fermi level. This is less than the $100\,\%$ expected for an ideal half metal, but close to the values measured in other Heusler half-metals in thin film form. Further evidence of half-metallicity comes from the spontaneous Hall angle, more than an order of magnitude higher than that observed in the $3d$-transition metals. This and the linear variation of m with x provided strong indications that $Mn_2Ru_{0.5}Ga$, grown by Kurt et al. [9] was a CFHM.

However, despite the experimental evidence, the measurements do not match the theoretical understanding of Mn_2Ru_xGa provided by Galanakis et al.[12]. There are three main areas where disagreement between theory and experiment exists, namely 1) the onset of half-metallicity; 2) the cell volume; and 3) the dependence of M on x.

Half-metallicity Density functional theory (DFT) investigations of $Mn_2Ru_{0.5}Ga$ indicate that, although it

This is an uncorrected manuscript. Please contact donald.maclaren@glasgow.ac.uk for a copy of the final version.

2

#	4a	4c	4b	4d	ΔH [eV]	M [μ_B]	c/a	Vol [Å^3]
1	Mn	Ru	Ga	Ru	-1.11	2.18	1.0	56.33
2	Ga	Mn	Ga	Ru	-0.99	2.93	1.0	55.83
3	Mn	Mn	Ga	Ru	-0.97	0.07 [a]	1.2	55.88
4	Mn	Mn	Ga	Ru	-0.52	4.66 [b]	1.0	55.01
⋮	⋮	⋮	⋮	⋮	⋮	⋮	⋮	⋮
10	Ga	Mn	Ga	–	0.02	3.14	1.0	52.01
12	Ru	Mn	Ga	–	0.27	0.19	1.0	44.70
13	Ru	Mn	Ga	Ru	0.29	4.44	1.0	59.20
14	–	Mn	Ga	Ru	0.52	4.50	1.0	49.60
15	Mn	Mn	Ga	–	0.54	0.47	1.0	46.54
⋮	⋮	⋮	⋮	⋮	⋮	⋮	⋮	⋮

[a] Magnetization quenched by the tetragonal distortion.
[b] Ferromagnetic Mn$_2$RuGa phase.

TABLE I: Calculated enthalpies of formation, ΔH, for the most stable competing Heusler phases of the 1221 structural and magnetic Mn-Ru-Ga cells investigated. The configurations investigated are limited to the primitive 4-atom Heusler cell (3-atom for half-Heuslers).[15]

may be possible to engineer a phase with zero magnetic moment, this will not be half-metallic [3, 5, 12]. Our calculations and those of others [12] find that the spin gap in the density of states (DOS) of Mn$_2$Ru$_{0.5}$Ga lies about 0.4 eV above the Fermi level, E_F. In Fig. 1 we plot the calculated DOS and the corresponding resistivity, obtained by solving the Boltzmann equations in the relaxation time approximation. Although the DOS exhibits a large spin polarisation, $\approx 60\%$, this is not reflected in that of the resistivity, which is only 30 %. Since our transport calculations are expected to overestimate the spin polarization, the presence of the 'pseudo-gap'[14] cannot justify the large experimentally observed spin polarization of the current.

Cell volume X-ray diffraction (XRD) and transmission electron microscopy (TEM) demonstrate that the films grow epitaxially with the in-plane lattice parameter being dictated by the MgO substrate ($a_{MRG} = \sqrt{2}a_{MgO}$) for all film thicknesses grown, while the out-of-plane lattice parameter c, depends strongly on the film thickness [10]. This results in cell volumes much larger than those predicted by DFT; and their variation with film thickness cannot be explained.

Magnetism The measured magnetic moment as a function of Ru concentration is linear[9] for $0.3 \leq x \leq 0.7$ with slope $dM/dx = 2$, suggesting that there is a spin gap at the Fermi level over an extended range of concentrations, in contradiction to the DFT results.

Here we address and resolve the conflict between experiment and theory. By applying a high-throughput approach based on the VASP[16] implementation of DFT and the Perdew-Burke-Ernzerhof (PBE)[17] functional, we have calculated the properties of 1221 Heusler phases containing Mn, Ru and Ga, that present different stoichiometry, magnetic order and site occupancy within the L2$_1$ and C1$_b$ symmetries. Other symmetries were excluded from the search. For each configuration we compute the enthalpy of formation, ΔH, with respect to the lowest energy phase of each of the constituent elements, allowing us to compare the relative stability of the various configurations. Our results for the lowest energy structures are summarized in Table I.

For the Mn$_2$RuGa composition, we find that the lowest energy structure corresponds to Mn occupying the inequivalent 4a, 4c sites, Ga the 4b and Ru taking the remaining 4d site, consistent with literature[4, 9]. Cubic Mn$_2$Ga was found to have a positive enthalpy of formation of 0.54 eV $f.u.^{-1}$, making the compound unstable with respect to decomposition into its elementary phases. The symmetry of the stable D0$_{22}$ structure was excluded from our calculations. However, the most energetically favourable Mn$_2$Ga structure in the L2$_1$ phase (# 15), places Mn on the inequivalent 4a and 4c sites with Ga occupying the 4b site. The structure remains cubic and the magnetic state is ferrimagnetic, consistent with experimental characterisation presented by Kurt et al. [9] for thin films stabilized on a suitable substrate or a seed layer. We note that the formation of any half-Heusler in the Mn, Ru and Ga phase diagram is energetically unfavourable, so that we would not expect pure half-Heuslers to be a significant constituent of the films.

We note that the energy of the system can be lowered by forming Mn-deficient MnRu$_2$Ga or MnGa$_2$Ru (# 1 and 2 in table I). Given that the difference in formation enthalpy of these phases with respect to Mn$_2$RuGa (# 3 in table I) is only 0.14 eV $f.u.^{-1}$, we expect that actual samples will not form distinct polycrystalline phases, but instead display significant site disorder, particularly on the 4a site, with a preference towards a lower Mn content. This was confirmed by laser-assisted inductively coupled mass spectroscopy (ICPMS) measurements of the Mn-to-Ga ratio for a series of samples with varying Ru concentration, x. The ratio was observed to be in the 1.6-1.9 range, increasing with increasing film thickness.

In Fig. 2 (a) we show scanning transmission electron microscopy (STEM) measurements of electron-transparent lamellæ of Mn$_2$RuGa which indicate that there is little variation in either the in-plane or out-of-plane lattice constants throughout the film. The corresponding electron energy loss (EELS) spectra and line profiles are shown in Fig. 2 (b). Alternating light and dark bands in dark-field images indicate slight compositional variations, especially in the layers closest to the surface. EELS measurements reveal that these bands correspond to layers of Mn enrichment and Ru depletion, suggesting a degree of phase segregation during growth, but not at the level of formation of half-Heuslers. We also note that the Ru concentration, x, decreases by about 20 % from the interface with the substrate through the thickness of the film; to a lesser extent, the Mn concen-

This is an uncorrected manuscript. Please contact donald.maclaren@glasgow.ac.uk for a copy of the final version.
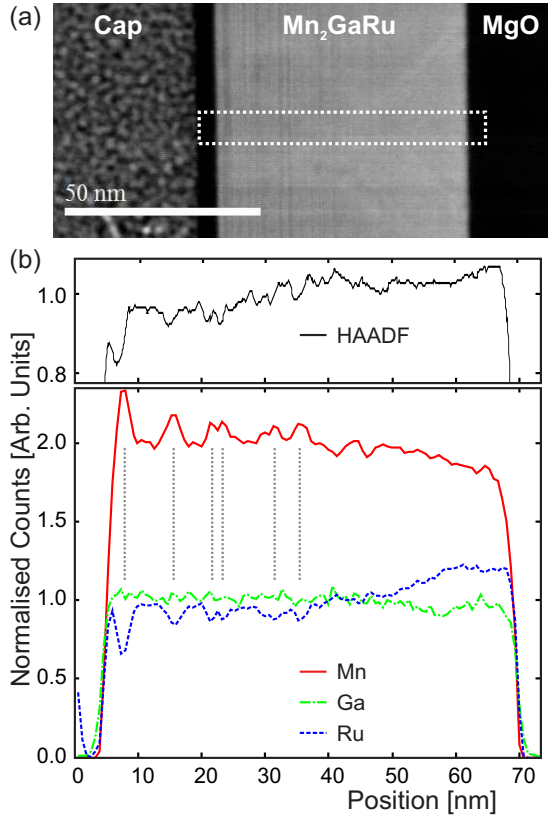
3

FIG. 2: Analytical electron microscopy analysis of the thin film ($x = 1$) composition. (a) High angle annular dark field (HAADF) image of a typical sample cross-section, with the region where EELS data were acquired indicated by a white rectangle. In HAADF images, heavy elements appear brightest. (b) Elemental variations across the thin film stack, as measured by EELS. Data are normalised by setting the average composition to Mn$_2$GaRu. The dashed vertical lines indicate regions where of Mn enrichment and Ru depletion, corresponding to darker features in the HAADF image.
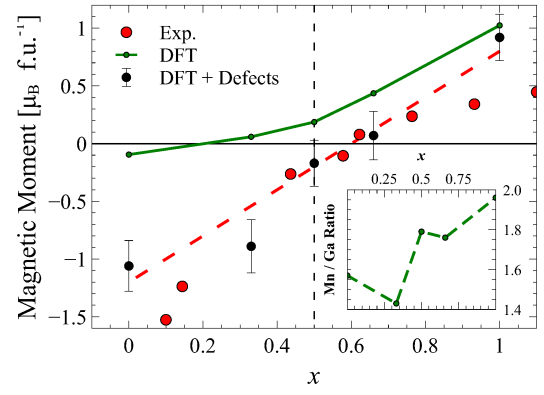

FIG. 3: Comparison of the magnetic moment predicted by DFT with the experimental results. The calculated magnetic moment for ideal MRG compounds is shown by the green line. Correction to the DFT magnetization due to the formation of Ga defects is shown by the black points. The corresponding estimate of the Mn/Ga ratio is shown in the inset. The dashed line equivalent to doping of $2\,e/$Ru is shown to guide the eye.

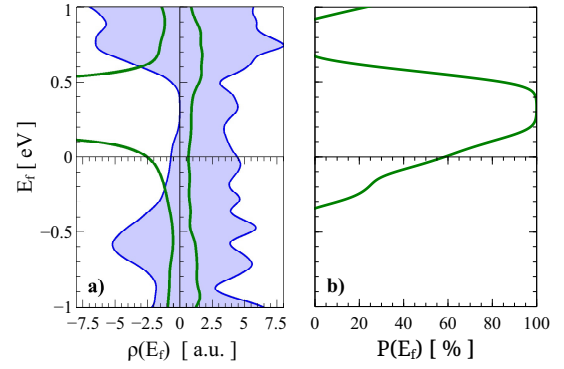FIG. 4: a) Spin resolved resistivity (green line) and the corresponding DOS (blue shadowed area) for electron-doped Mn$_2$Ru$_{0.5}$Ga. The doping was fixed at 0.4 electrons per formula. The data corresponding to the spin down channel are represented by negative values. b) Calculated transport spin polarization.

tration increases across the same range.

In order to investigate the properties of low-Mn-content films we have performed supercell calculations where $1/3$ of the Mn atoms at the $4a$ site are substituted with Ga. The Mn-Ga substitution simultaneously changes the lattice parameters, the magnetic properties and the electronic structure of the system. We find that the ionic charges of Mn and Ga are $+2$ and $+1$, respectively. Hence a one-atom Mn-Ga substitution leaves the system with one unbound electron, thus creating electronic doping. Below we describe in detail the properties of such Mn-deficient compounds.

Lattice Electronic doping provides an explanation for the variation of the lattice parameter with film thickness. From the volume difference between the relaxed DFT structure and the corresponding experimental one and by using the bulk modulus B_0, we estimate the experimental electronic doping. The bulk modulus is calculated for Mn$_2$Ru$_x$Ga ($x = $ 0.0, 0.33, 0.50, 0.66 and

1.0) compounds by fitting the Murnaghan equation of state[18, 19]. By using a simple model

$$n_{\mathrm{el}} = \frac{B_0}{S_0} \left[\left(\frac{c}{a}\right)_{\mathrm{exp}} \cdot \left(\frac{a_{\mathrm{exp}}}{a_0}\right)^3 - 1 \right] \ , \qquad (1)$$

we can relate the experimentally observed lattice parameters to the electron doping level, n_{el}. In Eq.(1) S_0 is the rate of change of the excess pressure with electron doping, while a_{exp} and a_0 correspond to the experimental in-plane lattice constant and the relaxed theoretical lattice constant, respectively. This equation is easily derived under the assumption that the material is in mechanical equilibrium at the experimental lattice constant, due to the excess pressure provided by the Mn-Ga substitution, via the electron doping mechanism. Since we are

comparing pressure differences, we ignore constant pressure terms. In order to stabilise the experimental lattice parameters, including the observed $c/a > 1$, we find electron doping in the range $0.1\,e\,f.u.^{-1}$ to $0.5\,e\,f.u.^{-1}$, corresponding to a Mn/Ga ratio in the interval 1.4 to 2.0. The higher doping level occurs for the lower Ru concentrations, as shown in the inset of Fig. 3.

TEM imaging and spectroscopy clearly indicate that there are regions of high Mn content, and therefore regions of enhanced Ga content elsewhere in the sample. It is therefore reasonable to assume that films of different thicknesses will have a different electronic doping, which in turn alters the c-lattice parameter and does so uniformly throughout the sample.

Magnetism A key feature of a CFHM is the magnetically compensated ground state. In agreement with Ref. [12], we find that the magnetization calculated for MRG compounds, as a function of the Ru doping, differs from the experimental one (see Fig. 3). The discrepancy is two-fold: I) the slope of the magnetization with x disagrees by a factor of 2, and II) there is no compensation of the magnetization around $x = 0.5$. These discrepancies are resolved if we take into account the effect of the Mn-Ga substitution on the magnetic properties. Ga defects introduce, in addition to the electronic doping, a change in the net magnetic moment per unit cell, of $-2\,\mu_{\mathrm{B}}$ per Mn substituted by Ga, which allows us to express the expected moment M_{EXP} as

$$M_{\mathrm{EXP}}(x) = M_{\mathrm{DFT}}(x) - 2 \cdot n_{\mathrm{el}}(x)\,, \qquad (2)$$

where M_{DFT} is the theoretically calculated magnetic moment for a defect-free $\mathrm{Mn_2Ru_xGa}$ compound.

The corrections given by Eqns. (1) and (2) have been applied for each value of x, and the results are summarised in Fig. 3. Notably, the presence of defects improves significantly the agreement between the experimental and theoretical magnetic moments, with the exception of concentrations around $x = 1$. A neutron diffraction study by Hori et al. [4] has shown that the magnetization of stoichiometric $\mathrm{Mn_2RuGa}$ ($x = 1$) is $\approx 1\,\mu_{\mathrm{B}}$, in good agreement with our calculations. This leads us to the conclusion that in the $x = 1$ limit there may be a substantial content of the $\mathrm{Ru_2MnGa}$ phase, which is known to be antiferromagnetic [4].

Electronic Structure Finally, we discuss the effect of the electronic doping on the degree of transport spin polarisation. In figure 4 we show the DOS and corresponding Boltzmann resistivity for $\mathrm{Mn_2RuGa}$ with $n_{\mathrm{el}} = 0.4$ extra electrons per formula unit, corresponding to a Mn/Ga ratio of 1.6 as observed by ICPMS. The additional doping results in a transport spin polarization of $\approx 60\,\%$, which is twice as large as the one calculated for the original $\mathrm{Mn_2Ru_xGa}$ compound. At a doping level of $n_{\mathrm{el}} = 1.0$ the transport spin polarization becomes $100\,\%$. It is important to note that the calculations presented here do not take into account the effect of the disorder

due to the Mn-Ga substitution on the transport properties. The stoichiometry has been shown to vary across the film as shown in figure 2, we would therefore expect a variation of the electronic structure which will in turn reduce the spin-gap.[12] However, the robustness of the experimentally observed spin-polarization can only be rationalized if a wide enough disorder-induced transport spin gap exists at the Fermi level. Disorder introduces a smearing to the band picture reducing conductivity in both spin channels through Anderson localization.[20] Localization of the states originates at the band edge, leaving the center of the band delocalized.[21] In MRG the Fermi level lies at the edge of the of the majority spin-band whereas for the minority it is at the band center. We would therefore expect that localization to affect the conductivity of the majority spin channel more than the minority resulting in an increased transport spin-polarization. Chadov *et al.* has demonstrated that this mechanism is applicable in the $\mathrm{Mn_{3-x}Co_xGa}$ system.[22]

Ideal half-metallicity exists only in the zero-temperature limit, and in the absence of spin-orbit interaction. Compensation for practical materials under ambient conditions occurs at a specific temperature, which can be tuned by composition and strain, while maintaining the Fermi level in the spin gap. This can be achieved because, unlike an antiferromagnet, the two magnetic sublattices have different temperature dependences [7, 11].

In conclusion, a sustained dialogue between experimental measurements and theoretical calculations have demonstrated that $\mathrm{Mn_2Ru_xGa}$ can form a true CFHM. As a consequence we expect that it will become a cornerstone for future spintronics technology. By means of high-throughput calculations, we have shown that there are several competing phases in the Mn-Ru-Ga system; and that due to their small energy differences they exhibit a strong tendency towards site disorder, and a preference for reduced Mn content. This has all been confirmed by our experimental characterization of MRG thin films. Furthermore the low Mn content provides an electronic doping mechanism, pushing the system towards half-metalicity and improving the agreement between experiment and theory regarding the structural and magnetic properties of the system. Based on our calculations, complete transport spin polarisation can be achieved.

We have shown that chemical composition, c/a ratio, tendency to site-disorder and cell volume are all correlated. To achieve transport half-metallicity and zero net moment, a reduced Mn to Ga ratio of ≈ 1.4 is required, as well as a Ru concentration of ≈ 0.7. Fine-tuning of the position of the Fermi level in the spin gap can then be achieved through varying the c/a ratio, which we have shown can be done by varying the film thickness.

This is an uncorrected manuscript. Please contact donald.maclaren@glasgow.ac.uk for a copy of the final version.

5

---

* archert@tcd.ie; www.materials-mine.com

[1] H. Van Leuken and R. A. De Groot, Phys. Rev. Lett **74**, 1171 (1995).

[2] M. Hakimi, M. Venkatesan, K. Rode, K. Ackland, and J. M. D. Coey, J. Appl. Phys. **113**, 17B101 (2013).

[3] L. Yang, B. Liu, F. Meng, H. Liu, H. Luo, E. Liu, W. Wang, and G. Wu, J. Magn. Magn. Mater. **379**, 1 (2015).

[4] T. Hori, M. Akimitsu, H. Miki, K. Ohoyoama, and Y. Yamaguchi, Appl. Phys. A-Mater. **74**, s737 (2002).

[5] S. Wurmehl, H. C. Kandpal, G. H. Fecher, and C. Felser, J. Phys.-Condens. Mat. **18**, 6171 (2006).

[6] I. Galanakis, P. Mavropoulos, and P. H. Dederichs, J. Phys. D Appl. Phys. **39**, 765 (2006).

[7] E. Şaşıoğlu, Phys. Rev. B **79**, 100406 (2009).

[8] X. Hu, Adv. Mater. **24**, 294 (2012).

[9] H. Kurt, K. Rode, P. Stamenov, M. Venkatesan, Y.-C. Lau, E. Fonda, and J. M. D. Coey, Phys. Rev. Lett. **112**, 027201 (2014).

[10] N. Thiyagarajah, Y.-C. Lau, D. Betto, K. Borisov, J. M. D. Coey, P. Stamenov, and K. Rode, Appl. Phys. Lett. **106**, 122402 (2015).

[11] D. Betto, N. Thiyagarajah, Y.-C. Lau, C. Piamonteze, M.-A. Arrio, P. Stamenov, J. M. D. Coey, and K. Rode, Phys. Rev. B **91**, 094410 (2015).

[12] I. Galanakis, K. Özdoğan, E. Şaşıoğlu, and S. Blügel, J. Appl. Phys. **116**, 033903 (2014).

[13] I. Galanakis, P. H. Dederichs, and N. Papanikolaou, Phys. Rev. B **66**, 134428 (2002).

[14] T. Timusk and B. Statt, Rep. Prog. Phys. **62**, 61 (1999).

[15] http://www.materials-mine.com.

[16] G. Y. Sun, J. Kürti, P. Rajczy, M. Kertesz, J. Hafner, and G. Kresse, J. Mol. Struc.-Theochem **624**, 37 (2003).

[17] J. P. Perdew, K. Burke, and M. Ernzerhof, Phys. Rev. Lett. **78**, 1396 (1997).

[18] C. L. Fu and K. M. Ho, Phys. Rev. B **28**, 5480 (1983).

[19] F. D. Murnaghan, **30**, 244 (1944), PMC1078704.

[20] P. W. Anderson, Phys. Rev. **109**, 1492 (1958).

[21] B. Kramer and A. MacKinnon, Reports on Progress in Physics **56**, 1469 (1993).

[22] S. Chadov, J. Kiss, and C. Felser, Adv. Funct. Mater. **23**, 832 (2013).